Icarus xxx (2010) xxx–xxx

Contents lists available at ScienceDirect

Icarus

journal homepage: www.elsevier.com/locate/icarus

An ensemble Kalman filter data assimilation system for the martian atmosphere: Implementation and simulation experiments

Matthew J. Hoffman [a,*], Steven J. Greybush [b], R. John Wilson [c], Gyorgyi Gyarmati [d], Ross N. Hoffman [e], Eugenia Kalnay [f], Kayo Ide [g], Eric J. Kostelich [h], Takemasa Miyoshi [b], Istvan Szunyogh [d]

[a] Earth and Planetary Sciences Department, Johns Hopkins University, 301 Olin Hall, 3400 N Charles St., Baltimore, MD 21218, United States
[b] Department of Atmospheric and Oceanic Science, University of Maryland, College Park, MD 20742, United States
[c] NOAA/Geophysical Fluid Dynamics Laboratory, P.O. Box 308, Princeton, NJ 08542, United States
[d] Department of Atmospheric Sciences, Texas A&M University, 3150 TAMU, College Station, TX 77843-3150, United States
[e] Atmospheric and Environmental Research, Inc., 131 Hartwell Avenue, Lexington, MA 02421, United States
[f] Department of Atmospheric and Oceanic Science, Institute for Physical Sciences and Technology, Earth System Science Interdisciplinary Center, University of Maryland, College Park, MD 20742, United States
[g] Department of Atmospheric and Oceanic Science, Center for Scientific Computation and Mathematical Modeling, Institute for Physical Sciences and Technology, Earth System Science Interdisciplinary Center, University of Maryland, College Park, MD 20742, United States
[h] Department of Mathematics and Statistics, Arizona State University, Tempe, AZ 85287, United States

ARTICLE INFO

Article history:
Received 3 September 2009
Revised 29 March 2010
Accepted 29 March 2010
Available online xxxx

Keywords:
Mars
Mars, Atmosphere
Atmospheres, Dynamics
Meteorology

ABSTRACT

The local ensemble transform Kalman filter (LETKF) is applied to the GFDL Mars general circulation model (MGCM) to demonstrate the potential benefit of an advanced data assimilation method. In perfect model (aka identical twin) experiments, simulated observations are used to assess the performance of the LETKF–MGCM system and to determine the dependence of the assimilation on observational data coverage. Temperature retrievals are simulated at locations that mirror the spatial distribution of the Thermal Emission Spectrometer (TES) retrievals from the Mars Global Surveyor (MGS). The LETKF converges quickly and substantially reduces the analysis and subsequent forecast errors in both temperature and velocity fields, even though only temperature observations are assimilated. The LETKF is also found to accurately estimate the magnitude of forecast uncertainties, notably those associated with the phase and amplitude of baroclinic waves along the boundary of the polar ice cap during Northern Hemisphere winter.

© 2010 Elsevier Inc. All rights reserved.

1. Introduction

With the increase in observational missions in the 1990s, data assimilation became a realistic option for studies of the martian atmosphere. The Mars Global Surveyor (MGS) in 1996, the Mars Odyssey in 2001, and the Mars Reconnaissance Orbiter in 2005 provide useful observational data sets of the martian atmosphere. However, coverage remains relatively sparse. The ability of data assimilation to estimate the state of an atmosphere based on sparse data sets using general circulation models (GCMs) makes it an extremely useful tool for the martian atmosphere. Data assimilation can produce a balanced (i.e., dynamically consistent) analysis field for all model variables (such as temperature and winds) using observations from only one or two observed fields (temperature, dust opacity) that are irregularly sampled in space and time. This paper discusses the assimilation of simulated temperature observations using the local ensemble transform Kalman filter (LETKF) of Hunt et al. (2007), a powerful and efficient assimilation scheme which has performed very well assimilating satellite observations in the terrestrial atmosphere (e.g., Szunyogh et al., 2005, 2008; Whitaker et al., 2008).

The potential benefit of data assimilation for Mars has been confirmed by a number of studies (Lewis and Read, 1995; Lewis et al., 1996, 1997, 2007; Houben, 1999) that have applied data assimilation to spacecraft observations. Banfield et al. (1995), one of the earliest studies, assimilated simulated observations using a Kalman filter approach, however, with a fixed covariance matrix, thereby foregoing the main advantage of the Kalman filter. Simulated observations were also used with the analysis correction scheme of Lorenc et al. (1991) (Lewis and Read, 1995; Lewis et al., 1996, 1997).

Assimilation efforts using real data have focused primarily on observations from the MGS spacecraft's Thermal Emission Spectrometer (TES). Between 1999 and 2005, during more than 25,000 polar orbits of Mars, the TES made hundreds of millions

* Corresponding author.
E-mail address: mjhoffman@jhu.edu (M.J. Hoffman).

0019-1035/$ - see front matter © 2010 Elsevier Inc. All rights reserved.
doi:10.1016/j.icarus.2010.03.034

Please cite this article in press as: Hoffman, M.J., et al. An ensemble Kalman filter data assimilation system for the martian atmosphere: Implementation and simulation experiments. Icarus (2010), doi:10.1016/j.icarus.2010.03.034

of IR radiance measurements of the martian atmosphere with a surface footprint size of approximately 3×3 km. These radiances have been used to derive vertical temperature profiles and dust opacity retrievals (Conrath et al., 2000; Smith et al., 2000, 2001). In turn, these atmospheric retrievals of temperature profiles (Houben, 1999; Zhang et al., 2001) and total dust optical depth (Lewis et al., 2007) have been used in assimilation studies with varying results.

Houben (1999) assimilated real TES temperature retrievals with a 4D-VAR scheme using an approximation of the tangent linear model instead of the full tangent linear model. The assimilation run was very short, but provided promising analyses of the zonal mean fields. TES temperature retrievals were also assimilated by Zhang et al. (2001) using the steady state Kalman filter of Banfield et al. (1995) with mixed results.

The UK Mars data assimilation system is currently the most comprehensive system in use. Both temperature and dust opacity retrievals from the TES were assimilated by Lewis et al. (2007) using the analysis correction scheme (Lorenc et al., 1991), which is a modification of the successive corrections method (SCM). Assimilating these retrievals was found to benefit the atmospheric analysis during a martian dust storm (Montabone et al., 2005; Lewis et al., 2007). A reanalysis of the martian atmosphere using this method provides the current best estimate of the state of the martian atmosphere during the MGS mission (Montabone et al., 2006).

Here, simulated retrievals of temperature are assimilated by the LETKF into the GFDL Mars GCM (MGCM). In the martian data assimilation studies described above, the assimilation methods used have been less advanced as compared to the methods currently used in terrestrial atmospheric data assimilation. One of the primary challenges in martian data assimilation is that observational data is extremely sparse. More advanced data assimilation methods, though, have been found to be more efficient in extracting information about the state of the atmosphere from such sparse data sets (e.g., Szunyogh et al., 2005, 2008; Whitaker et al., 2008). The present work demonstrates that the LETKF is accurate and robust when applied to an MGCM using simulated retrievals with a TES-like sampling pattern.

Section 2 describes the Mars model and Section 3 describes the ensemble Kalman filter methodology used in this study. Section 4 details the simulation experiments and Section 5 describes results from these experiments. Section 6 presents a summary and conclusions.

2. GFDL Mars general circulation model

The GFDL MGCM was originally based on the GFDL SKYHI terrestrial GCM and an early version of the model was described in Wilson and Hamilton (1996). Subsequent descriptions appear in Richardson and Wilson (2002) and Hinson and Wilson (2004). This model has been used to examine tides and planetary waves (Wilson and Hamilton, 1996; Hinson and Wilson, 2004; Wilson et al., 2002; Hinson et al., 2003), the water cycle (Richardson and Wilson, 2002; Richardson et al., 2002), the dust cycle (Basu et al., 2004, 2006; Wilson et al., 2008b) and cloud radiative effects (Hinson and Wilson, 2004; Wilson et al., 2007, 2008). More recently the physical parameterizations have been adapted to the GFDL Flexible Modeling System (FMS) which includes a choice of dynamical cores (finite difference, finite volume and spectral) and associated infrastructure. The Mars physics has been tested with all three dynamical cores. Here we elect to use the finite volume (FV) model.

The FV model employs a conservative flux-form semi-Lagrangian horizontal discretization with monotonic constraints (Lin and Rood, 1996, 1997), a physically consistent finite-volume integration of the pressure gradient force (Lin, 1997), and a terrain-following Lagrangian control-volume vertical coordinate that simplifies vertical advection calculations while maintaining high-order numerical accuracy (Lin, 2004). This core has been implemented with a latitude–longitude grid typical of most climate models and, more recently, on a cubed-sphere grid (Putnam and Lin, 2007). The calculations presented here employ the regular latitude–longitude grid structure with $5^\circ \times 6^\circ$ resolution in latitude and longitude (60 longitudes and 36 latitudes) and 28 levels in the vertical, extending from the surface to roughly 85 km.

The MGCM includes surface and subsurface physics which allow the calculation of realistic surface temperatures; a budget for gaseous and condensed CO_2 which yields a realistic annual cycle of global atmospheric mass; solar and infrared radiative transfer for both gaseous CO_2 and atmospheric aerosol (i.e., dust); aerosol transport which allows for a self-consistent simulation of the aerosol distribution; and a boundary layer parameterization. The model maintains mass-conserving inventories of water (regolith, surface frost, vapor and condensate) and dust mass (surface dust and aerosol, by particle size), which can be used for accounting where dust has been lifted and deposited on the surface.

Model input fields include topography, surface albedo, thermal inertia, and emissivity. Temporally and spatially varying column opacity and dust injection fields may also be input, depending on the needs of the experiment being carried out. These input fields are interpolated linearly in latitude and longitude to the appropriate model grid. The MGCM has a 12-layer soil model with a depth-dependent soil diffusivity that has been tuned to fit the observed TES surface temperatures (Wilson et al., 2007).

The model uses the radiation code developed by the NASA Ames Mars modeling group (Kahre et al., 2006, 2008). This code is based on a two-stream solution to the radiative transfer equation with CO_2 and water vapor opacities calculated using correlated-k values in 12 spectral bands ranging from 0.3 to 250 μm. The two-stream solution is generalized for solar and infrared radiation, with scattering based on the δ-Eddington approximation at visible wavelengths and the hemispheric mean approximation at infrared wavelengths (Toon et al., 1989). Aerosol heating rates are calculated by using the optical properties of the evolving aerosol size distribution (and composition) at both solar and infrared wavelengths. The dust composition is currently based on a "Mars dust" analog in the visible (Ockert-Bell et al., 1997) and the IR description is based on fits to TES spectra carried out by Wolff and Clancy (2003). The radiation code utilizes tables of optical properties (particle extinction, single scattering albedo and asymmetry factor) tabulated from Mie theory calculations for both bare and ice-coated dust particles.

In the simulations described here, we prescribe a spatially uniform distribution of dust with a column opacity of 0.3 when referenced to the 6.1 hPa pressure surface. Although more sophisticated descriptions exist and have been used in other studies, this simple, fixed dust distribution was chosen for simplicity in the initial studies. An evolving dust distribution (e.g. Wilson et al., 2008a) will be used in future studies.

3. Local ensemble transform Kalman filter

In a data assimilation scheme, an improved estimate of the current state is derived by combining current observations and a short-term forecast of the current state, which is created using prior information and is referred to as the "background". The improved state estimate, hereafter called the "analysis", is then used as the initial condition for the model, which, in turn, creates a new forecast at a future time (Fig. 1). Data assimilation proceeds in this manner, alternating between a forecast step, where the model predicts the future state of the system, and an analysis step, where

Please cite this article in press as: Hoffman, M.J., et al. An ensemble Kalman filter data assimilation system for the martian atmosphere: Implementation and simulation experiments. Icarus (2010), doi:10.1016/j.icarus.2010.03.034

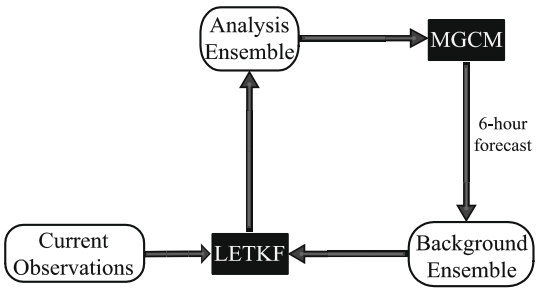

Fig. 1. A diagram of the data assimilation workflow.

observations taken at this future time are incorporated and the analysis is created. Both the background and the observations have errors, and the analysis step consists of a statistical procedure that takes these errors into account in determining the analysis state.

The data assimilation scheme used here is the LETKF of Hunt et al. (2007) and the implementation is available at http://math.-la.asu.edu/~eric/letkf/index.html. The LETKF is an approximation of the Kalman filter and as such seeks an analysis solution with minimum error variance. As with all ensemble Kalman filters, the LETKF uses an ensemble of k model states to characterize the uncertainty of the forecast. These ensemble members are model states valid at the same time, which differ only in the initial conditions used for the model run. In the following equations, the state vectors, $\mathbf{x}^{(i)}$, $i = 1, \ldots, k$, are column vectors which contain all of the model prognostic variables (temperature and winds). The ensemble forecasts (or background) fields, denoted $\mathbf{x}^{b(i)}$, are created by integrating the model forward for 6 h (i.e., 0.25 sols, since 24 martian hours equals one sol) from the previous analysis ensemble. The state space vectors $\mathbf{x}^{b(i)}$ are then transformed into observation space vectors $\mathbf{y}^{b(i)} = H(\mathbf{x}^{b(i)})$ using the observation operator, H. In this paper, the observed variable (temperature) is a model variable and the observations are simulated at grid points, so H does not involve interpolation or a conversion from model to observed variables.

The LETKF used here is localized by considering only the observations within a prescribed horizontal and vertical distance. A trapezoidal taper is used in the horizontal, while a boxcar (step function) taper is used in the vertical. A trapezoidal taper gives weight 1 to all observations inside of a specified inner distance and then linearly decreases the weights out to an outer distance while a boxcar taper gives weight 1 to all observations within a single specified distance. The algorithm compiles all of the information in a given region initially and then the analysis at each grid point is computed independently. In the equations that follow, the state and observation vectors are local vectors containing only the information in the local neighborhood of the analysis point.

The background state is defined as the mean of the background ensemble,

$$\mathbf{x}^b = k^{-1} \sum_{i=1}^{k} \mathbf{x}^{b(i)}, \tag{1}$$

and the background covariance in state space is given by

$$\mathbf{P}^b = (k-1)^{-1} \mathbf{X}^b (\mathbf{X}^b)^T = (k-1)^{-1} \sum_{i=1}^{k} (\mathbf{x}^{b(i)} - \mathbf{x}^b)(\mathbf{x}^{b(i)} - \mathbf{x}^b)^T, \tag{2}$$

where $\mathbf{X}^b$ is defined as the matrix whose ith column is $\mathbf{x}^{b(i)} - \mathbf{x}^b$, where $\mathbf{x}^b$ is the ensemble average. The background covariance, however, is not explicitly computed in the LETKF. Instead, the background perturbations, $\mathbf{X}^b$, are transformed into analysis perturbations, $\mathbf{X}^a$, using the symmetric square root of the analysis covariance in ensemble space:

$$\mathbf{X}^a = \mathbf{X}^b [(k-1)\widetilde{\mathbf{P}}^a]^{1/2}. \tag{3}$$

The analysis covariance in ensemble space is given by the equation

$$\widetilde{\mathbf{P}}^a = \left[(k-1)\mathbf{I} + \mathbf{Y}^{b^T} \mathbf{R}^{-1} \mathbf{Y}^b \right]^{-1}, \tag{4}$$

where $\mathbf{R}$ is the observation covariance matrix and $\mathbf{Y}^b$ is the matrix of background ensemble perturbations in observation space whose ith column is $\mathbf{y}^{b(i)} - \mathbf{y}^b$. Note that the matrix $\mathbf{Y}^b$ is created using the non-linear observation operator, as opposed to variational methods that require the Jacobian or adjoint of the observation operator.

To complete the data assimilation, the analysis ensemble mean state is determined by the equation

$$\mathbf{x}^a = \mathbf{x}^b + \mathbf{X}^b \widetilde{\mathbf{P}}^a \mathbf{Y}^{b^T} \mathbf{R}^{-1} (\mathbf{y}^o - \mathbf{y}^b), \tag{5}$$

and the new analysis is obtained by adding the analysis mean to each column of the analysis perturbation matrix $\mathbf{X}^a$. Please refer to Hoffman et al. (2008) for a succinct summary of the derivation of the above equations or to Hunt et al. (2007) for the full details. The grid point analysis ensembles are then gathered together to create the global ensemble analyses, which are used as initial conditions for the next cycle ensemble forecasts.

4. Simulated observations and experiment setup

To test the performance of the LETKF–MGCM system, "identical twin" experiments were conducted. In identical twin experiments, the "true" or "nature" state of the atmosphere is taken to be a single model forecast. The assimilation system then tries to approximate this "true" state beginning from different initial conditions. Since the "true" state is known, the performance of the system can be evaluated. Observations are generated by taking the long nature run used for validation, beginning during Northern Hemisphere winter ($Ls \sim 250$), and adding random Gaussian errors with a 3 K standard deviation to the temperature field. The assimilation experiment was started from sol 10 (martian day) of the nature run and assimilations were performed every 6 h at hours 00, 06, 12, and 18. Northern Hemisphere winter is used because traveling Rossby waves are found in the Mars atmosphere during that season (Banfield et al., 2004). During the Southern Hemisphere winter (NH summer) the Mars atmosphere is relatively quiescent.

Two separate observation distributions were used. No observations of winds are used in either distribution, but the estimates of the zonal and meridional winds provided by the background are updated by the LETKF based on the temperature observations. TES temperature profiles have been found to have an uncertainty of approximately 2 K and sometimes larger near the surface (Smith et al., 2001). In reality, the TES retrievals also have correlated errors, but here we have ignored this and instead we consider relatively large—3 K—random errors for both sets of observations. The first distribution has a simulated temperature observation at every grid point, which will be referred to as the "full coverage" observations. The motivation for using only temperature observations is the goal of eventually assimilating TES temperature retrievals. The full coverage distribution allows the assessment of the LETKF–MGCM system performance under ideal observation coverage. In the second distribution, called the "simulated TES" retrievals, the real TES retrievals from the previous 6 h are read into the system at every assimilation time and temperature retrievals are simulated at the grid points closest to the real retrievals but at the assimilation time. The TES temperature profiles are provided at fixed pressure levels, but, because the MGCM uses a hybrid vertical coordinate, the closest model level varies geographically and with time.

In the experiments described in this paper, 16 ensemble members are used and the covariance inflation factor that multiplies the background error covariance at each analysis time is prescribed as

Please cite this article in press as: Hoffman, M.J., et al. An ensemble Kalman filter data assimilation system for the martian atmosphere: Implementation and simulation experiments. Icarus (2010), doi:10.1016/j.icarus.2010.03.034

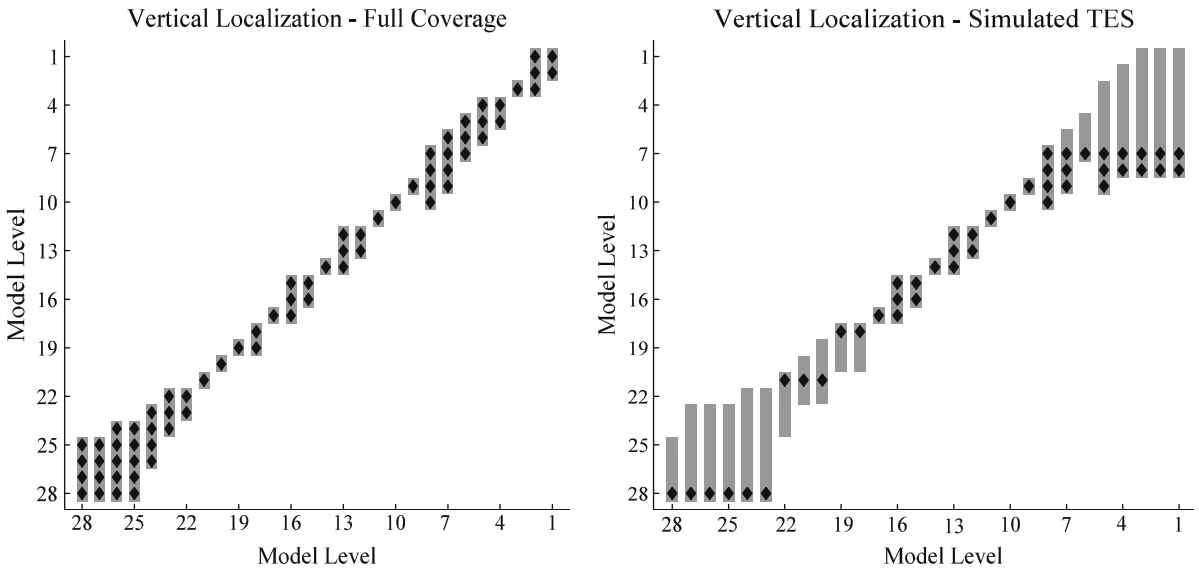

Fig. 2. Vertical levels used in the localization (bars) for each model level in the full coverage (left) and simulated TES (right) distributions. Observations for each of the distributions at each level are shown as diamonds.

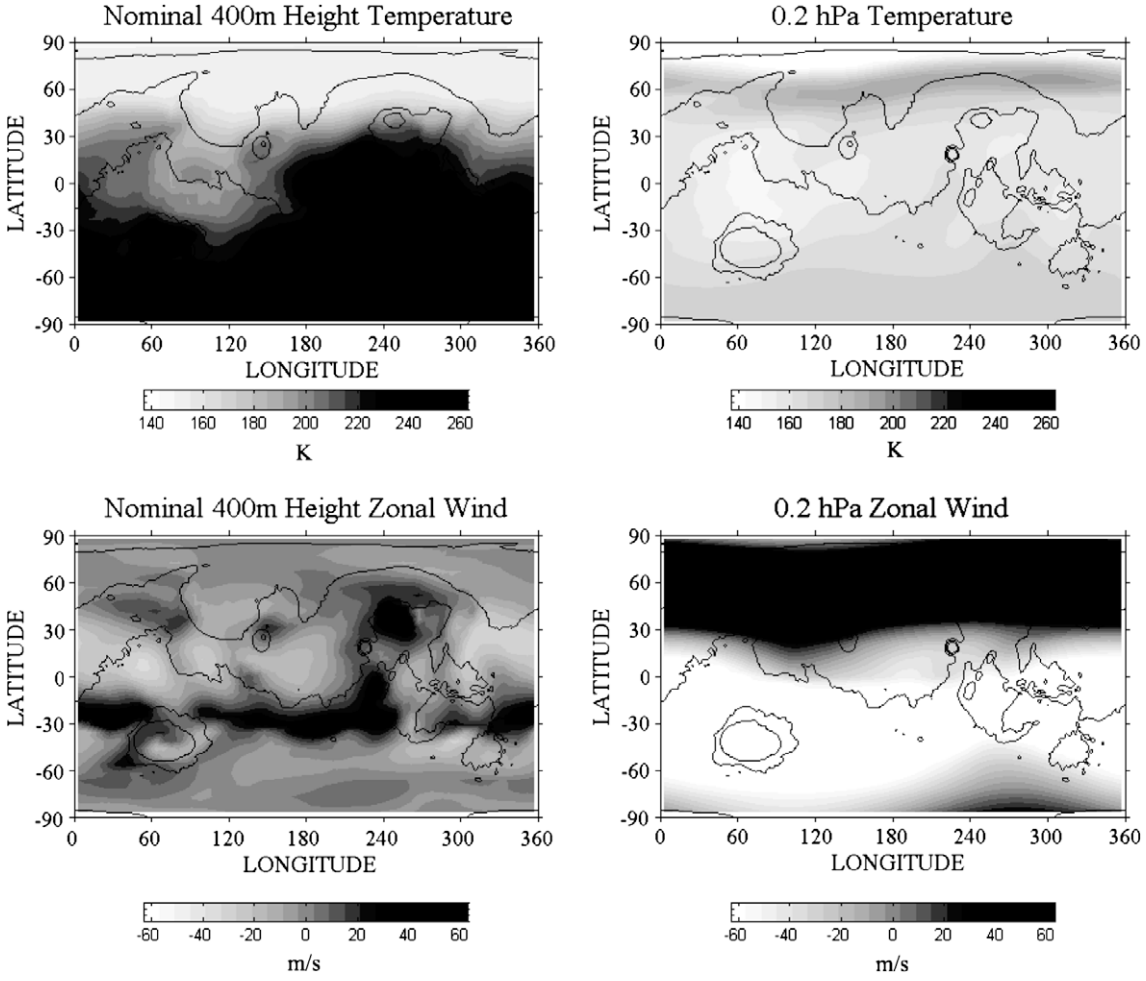

Fig. 3. Left: The temperature [K] and zonal component of the wind vector field [m/s] from sol 10 of the nature run (truth) at a nominal 400 m height above ground. The temperature at this height is largely determined by surface heating and the zonal wind has a weak jet at 30°S. Right: The temperature [K] and zonal component of the wind vector field [m/s] from the sol 10 of the nature run (truth) at 0.02 hPa. The temperature is smooth, except between 60°N and 90°N, while the zonal wind shows a strong jet between 30°N and 90°N.

Please cite this article in press as: Hoffman, M.J., et al. An ensemble Kalman filter data assimilation system for the martian atmosphere: Implementation and simulation experiments. Icarus (2010), doi:10.1016/j.icarus.2010.03.034

0.10. Here the covariance inflation accounts for imperfect assumptions such as model nonlinearities. In real data applications, covariance inflation must also account for the effect of model error. Experiments run with 40 ensemble members yielded a nearly identical result, which implies that the martian atmosphere may have lower-order dynamics than the more chaotic Earth atmosphere, for which ensembles of at least 40 members are common. The horizontal localization distance for this study is 1200 km, following the Lewis et al. (2007) assimilation study that used a radius of influence of 1200 km for observations. The horizontal localization distance is larger than the martian deformation radius of 920 km (Read and Lewis, 2004). A trapezoidal taper is used for the rectangular horizontal localization which gives weight 1 to all observations inside of 900 km and then linearly decreases the weights to zero at 1200 km.

Ensemble size, covariance inflation, observation error, and horizontal localization are held constant in experiments for both observation distributions used in this study, but the vertical localization parameters are varied based on the observation distribution. Vertical localization is set as a fraction of the atmospheric scale height and is varied by level. For the full coverage distribution of observations, the vertical localization allows the LETKF to use observations from one or two levels on either side. The simulated TES retrievals, however, have gaps of up to six model levels without a retrieved value, so a larger vertical localization radius is needed, particularly in the upper levels of the atmosphere. The vertical profiles derived from the TES retrievals have values at 19 pressure levels, compared with 28 model levels. When the TES pressure levels are mapped to the nearest model level of the MGCM, there are a few instances of more than one TES profile levels being closest to the same model level. As a result, instead of 19 profile levels, there are approximately 14 levels in a simulated TES profile. Furthermore, these levels are not evenly distributed throughout the model. The majority of the TES retrieval profiles are concentrated in the middle of the model grid between pressures of 4.76 hPa and 0.11 hPa (model levels 18 through 7). There are no TES retrievals higher than 0.11 hPa, so the upper six levels of the model have no observations. Fig. 2 shows the vertical observation distributions and the levels used in the localization for both experiments. There is no tapering used in the vertical, so all levels within the localization distance are given weight 1.

The experiment using full observational coverage corresponds to 57,120 temperature observations at every analysis time whereas the simulated TES distribution corresponds to only about 4300 retrievals per analysis or 7% of the full coverage. There are some analysis times with no retrievals due to data gaps caused by a variety of spacecraft operational issues. Longer gaps in the data (~20 days) occur when the orbiter is in solar occultation interrupting communication with Earth, although the data period used here does not contain an occultation.

To create the initial ensemble, the 16 model states from the previous four sols of the nature run were used. The LETKF–MGCM system was then run for a 55 sol period from $Ls \sim 256$ to $Ls \sim 292$, so all results correspond to Northern Hemisphere winter. As a benchmark, a long integration of the model was also carried out starting from the background (initial ensemble average) of the very first data assimilation step. Such an initial condition would not be on the attractor (i.e., dynamically consistent) at first, so it is expected that there will be an initial spin-down towards the attractor. The results from this run, called the free run forecast (FRF), represent the case where no observational information is injected into the state estimation process.

Since much of the variability during Northern Hemisphere winter is due to Rossby waves along the polar temperature front

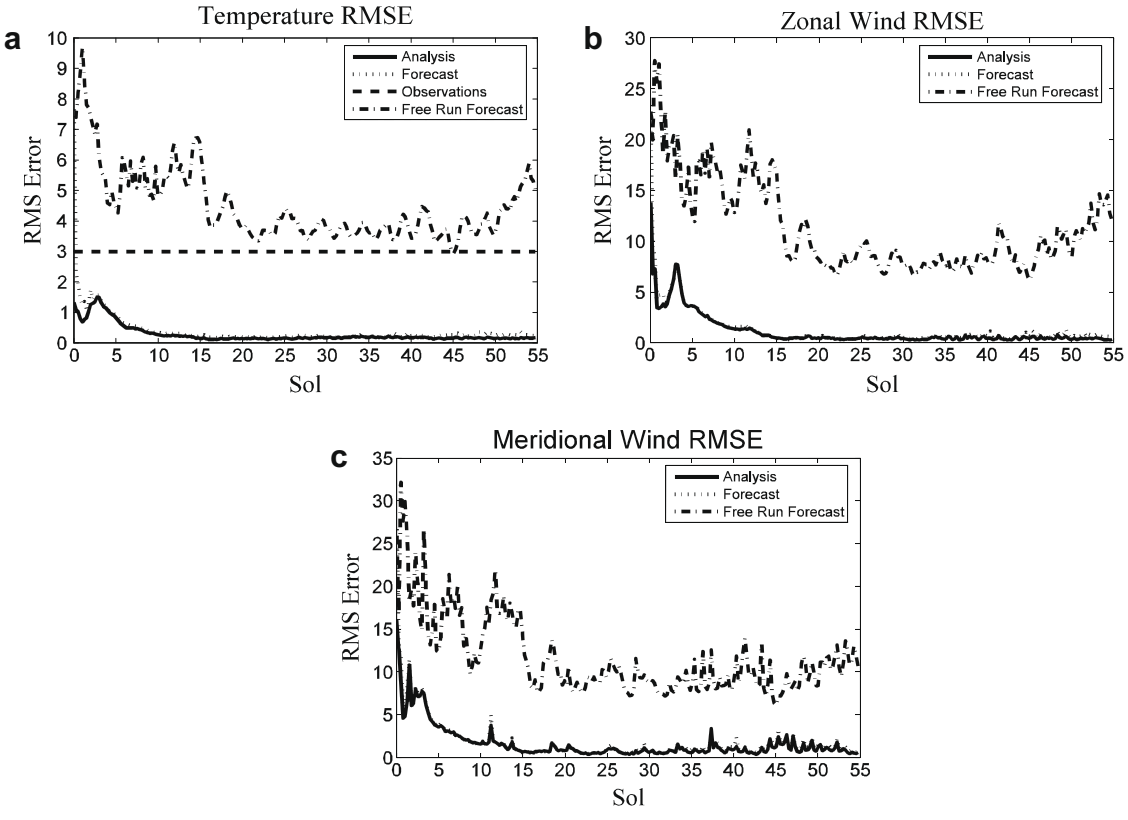

Fig. 4. (a) The RMS error north of 30°N in temperature [K] from an identical twin experiment using observations at every grid point with observation error of 3 K, a 1200 km horizontal localization radius, and 10% inflation. (b) The RMS error north of 30°N in zonal wind [m/s] of the same experiment. (c) The RMS error north of 30°N in zonal wind [m/s] of the same experiment. The analysis and forecast (i.e., background) are improved for the winds even though no wind observations are assimilated.

Please cite this article in press as: Hoffman, M.J., et al. An ensemble Kalman filter data assimilation system for the martian atmosphere: Implementation and simulation experiments. Icarus (2010), doi:10.1016/j.icarus.2010.03.034

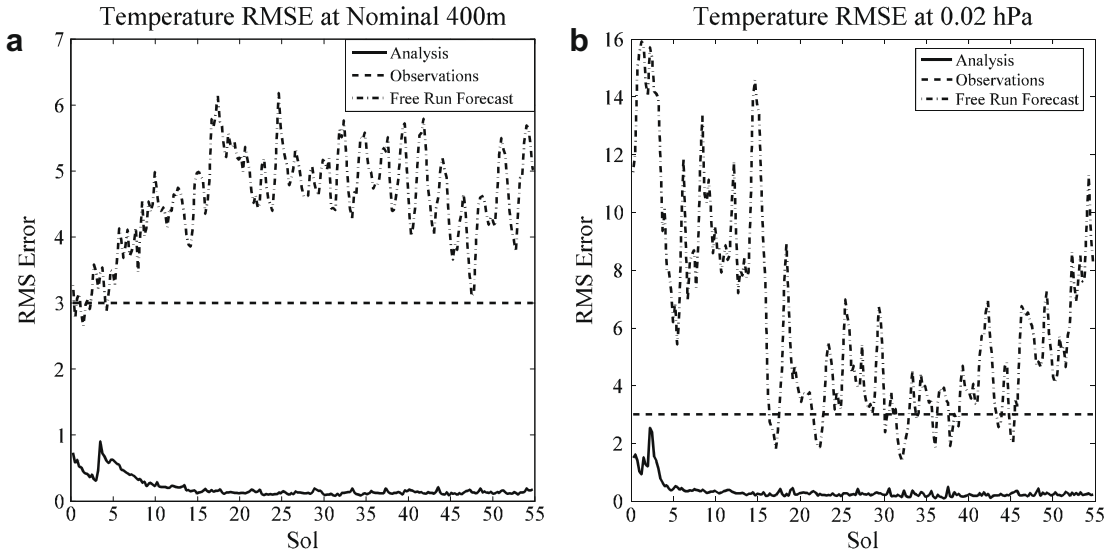

Fig. 5. (a) Time evolution of the root-mean-square error north of 30°N in the estimates of the temperature [K] by the free model run and the cycled data assimilation of temperature observations at a nominal height of 400 m above ground level. (b) Time evolution of the root-mean-square error north of 30°N in the estimates of the temperature [K] by the free model run and the cycled data assimilation of temperature observations at 0.02 hPa height.

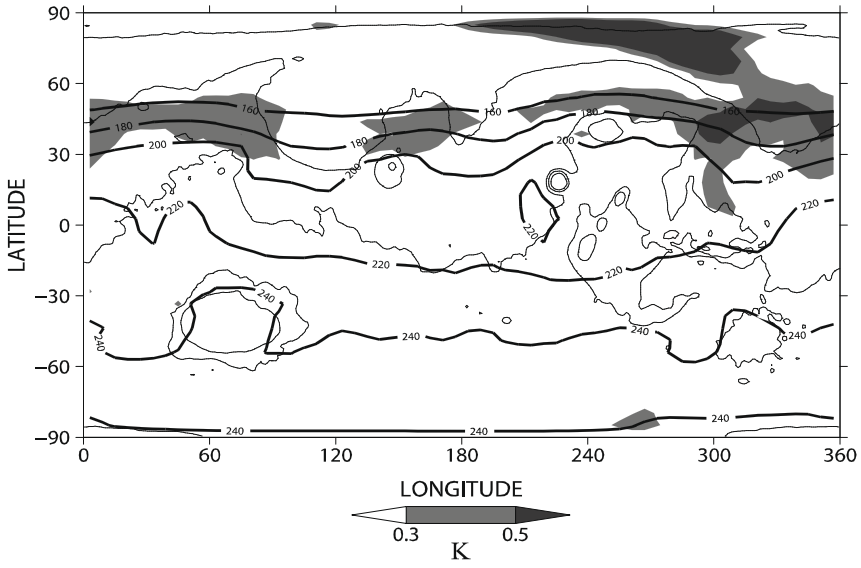

Fig. 6a. The RMS analysis error [K] (shaded) and average truth temperature field [K] (contour) from sol 2 to sol 21 of the experiment at a nominal height of 400 m above ground level using observations at every grid point with 3 K observation error, 10% inflation, and 16 ensemble members.

(Banfield et al., 2003, 2004), results here focus on the improvement provided by the analysis poleward of 30°N. Upper and lower levels of the MGCM exhibit different behavior in the free run forecast based on their different dynamics. In addition to vertically averaged results, results are shown for two levels: a nominal height of 400 m above ground level that is strongly affected by forcing of the atmosphere by solar surface heating and topography; and at 0.02 hPa in the free atmosphere that is characterized by a strong meridional temperature gradient and associated zonal wind jet. The difference between the atmospheric flow at the two levels is illustrated by showing the temperature and the zonal component of the wind at both levels in the nature run at a time when the model state is already settled on the model attractor after the initial transient phase of model behavior (Fig. 3). In Fig. 3 we see a strong diurnal temperature signal and a weak zonal wind jet around 30°S near the surface and a smooth temperature field and strong zonal jet in the free atmosphere. As a consequence, the analysis and FRF errors exhibit different behavior at the two levels as well.

5. Results

Using the full coverage observations, the LETKF–MGCM system quickly reduces the analysis and subsequent forecast root-mean-square (RMS) error for the temperature (Fig. 4a), zonal velocity (Fig. 4b), and meridional velocity (Fig. 4c). The state estimation error in the free run, started from the ensemble average of states taken at different times of the day, initially decreases with time (Fig. 4a) as the model equilibrates to the forcing of the diurnal cycle, which underscores the dominate role that diurnal forcing plays in the evolution of the Mars atmosphere dynamics, especially at near surface levels. Compared to the vertically averaged

Please cite this article in press as: Hoffman, M.J., et al. An ensemble Kalman filter data assimilation system for the martian atmosphere: Implementation and simulation experiments. Icarus (2010), doi:10.1016/j.icarus.2010.03.034

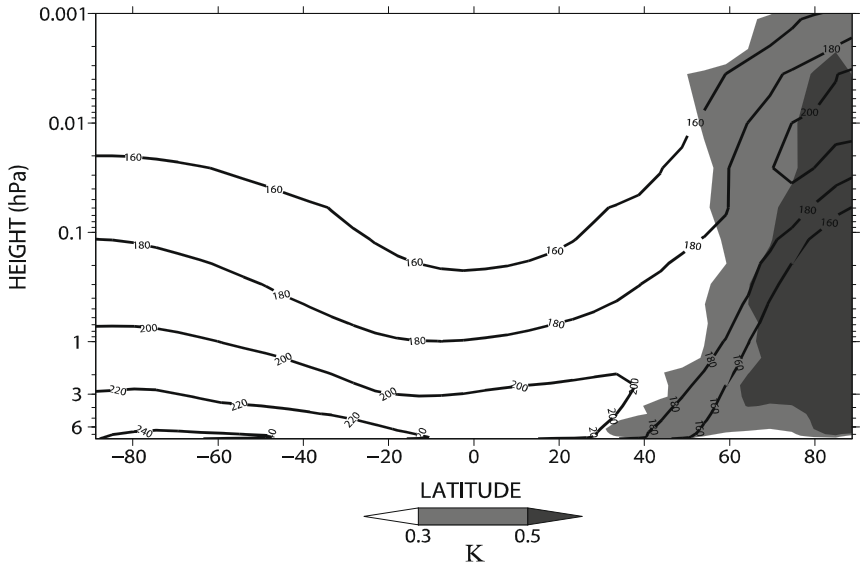

Fig. 6b. Vertical profile of the RMS analysis error [K] (shaded) and average truth temperature field [K] (contour) over the same period. The vertical axis is model level labeled by reference pressure in hPa, plotted with a log axis.

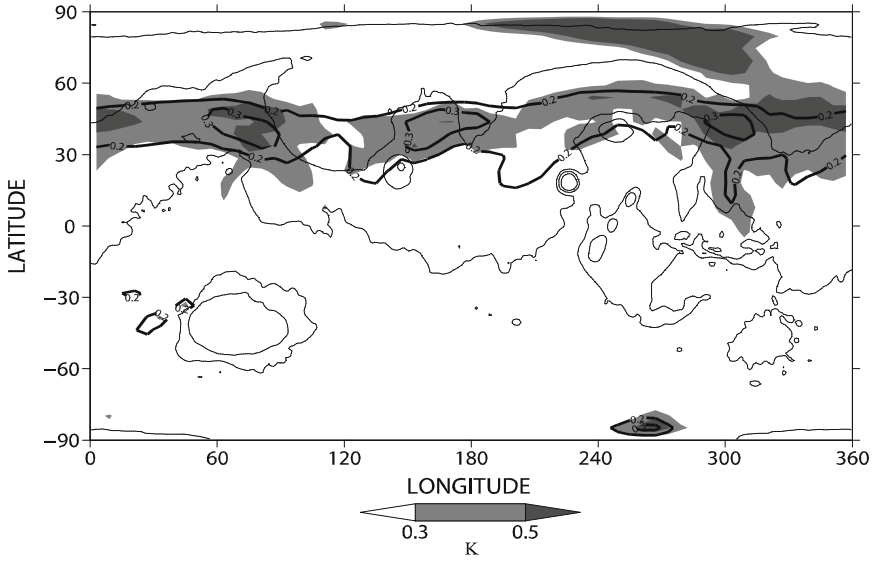

Fig. 7a. Background RMS error [K] (shaded) and background spread in temperature [K] (contour) averaged over the period from sol 2 of the simulation to sol 21 at a nominal height of 400 m above ground level using observations at every grid point with 3 K observation error, 10% inflation, and 16 ensemble members.

temperature analysis errors (Fig. 4a), greater variability is seen in the analysis of temperature at the lower and upper levels of the atmosphere (Fig. 5a and b) and in the velocity fields (Fig. 4b and c). In all of the fields, the data assimilation has a large positive influence on the accuracy of the state estimate. Compared to the FRF, the injection of observations within the LETKF accelerates the initial speed of the convergence and leads to a major reduction of the asymptotic value of the RMS error in the state estimate. In the meridional wind field, which is not directly observable from satellites, these improvements could provide a more accurate picture of the diabatic circulation.

There is a difference between the behaviors of the estimation errors at 0.02 hPa and nominal 400 m over the first 2–3 sols. Data assimilation leads to a quicker improvement in the lower levels and error remains relatively constant in time. In the upper atmosphere, where dynamics plays a relatively more important role compared to the diurnal surface forcing, there is more fluctuation initially before the RMS error approaches the asymptotic value at sol 5. The greater role of dynamics as opposed to forcing in the upper levels of the atmosphere can also be seen in the ensemble spread. Ensemble spread is larger above 0.4 hPa and below a nominal 400 m height above ground, while the forecast ensemble spread collapses quickly in between.

In the full coverage observation experiment, the largest analysis error is in the Northern Hemisphere in the lower levels. The RMS analysis error and the average temperature field show that the largest analysis error occurs along the sharp temperature gradient around 45°N at the boundary of the polar ice cap (Fig. 6a). The analysis error extends upwards in the vertical along this temperature front, which can be seen in the zonal average (Fig. 6b). The analysis error is extremely low in other regions. Analysis errors at around 45°N (Fig. 6) have the same horizontal and vertical

Please cite this article in press as: Hoffman, M.J., et al. An ensemble Kalman filter data assimilation system for the martian atmosphere: Implementation and simulation experiments. Icarus (2010), doi:10.1016/j.icarus.2010.03.034

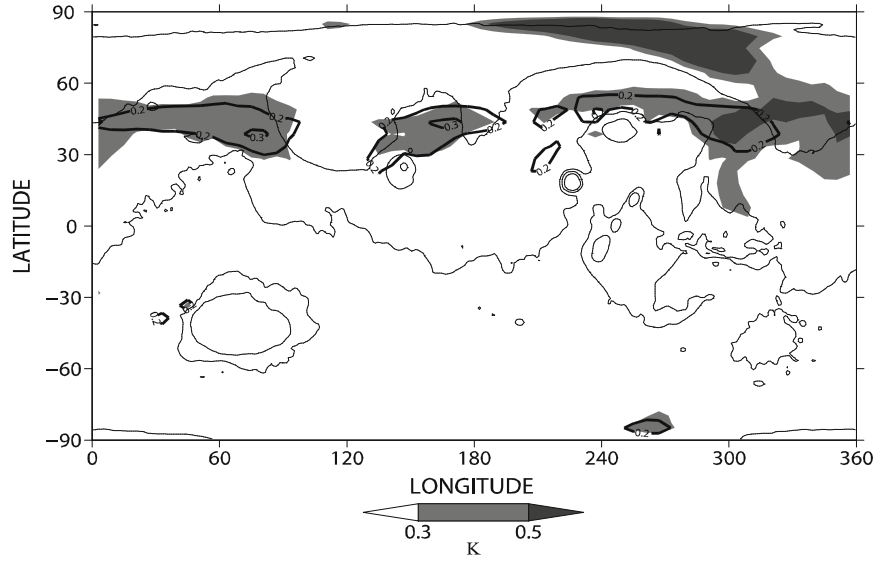

Fig. 7b. Analysis RMS error (shaded) and average analysis spread (contour) in temperature for the same experiment as (a).

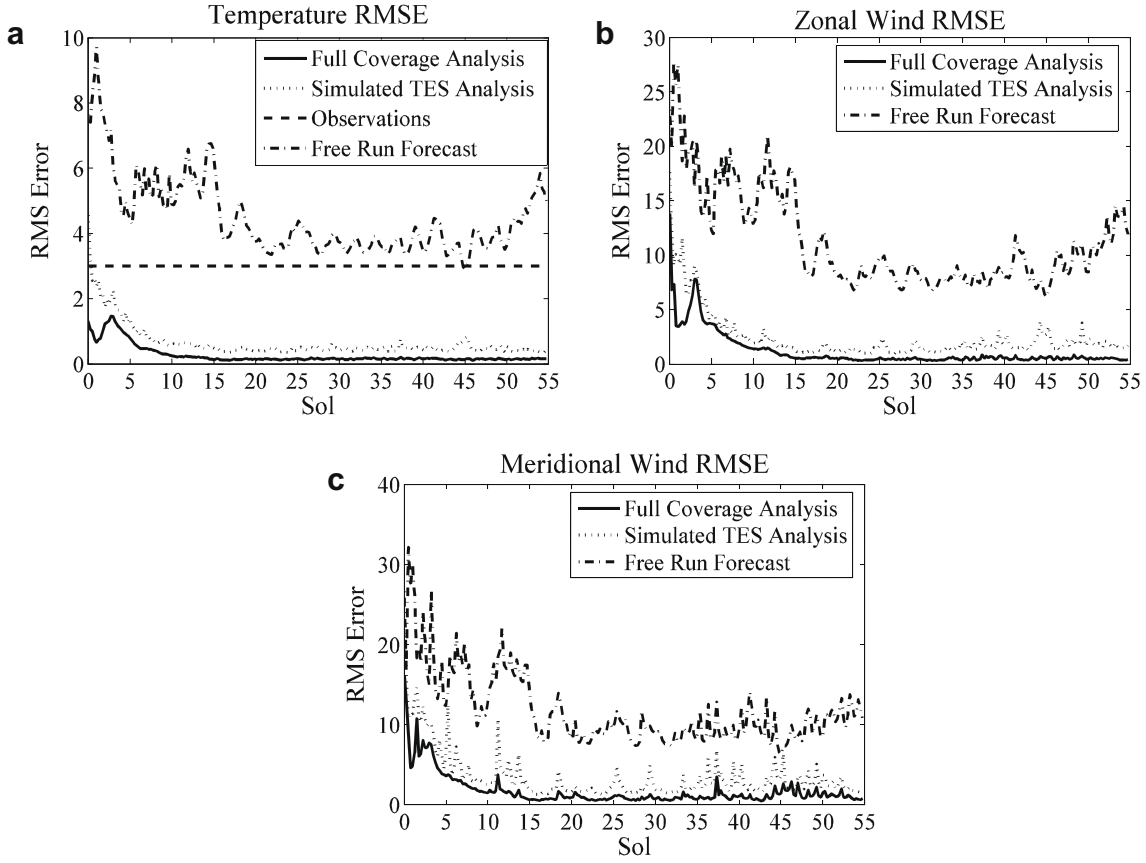

Fig. 8. (a) Comparison of the RMS error north of 30°N in temperature using full coverage observations (full coverage analysis) and simulated TES retrievals (simulated TES analysis). A 1200 km horizontal localization radius is used with an observation error of 3 K, 10% inflation, and 16 ensemble members. (b) Same comparison in zonal wind and (c) meridional wind.

signature as the strong baroclinic waves that have been observed in this region and season (Barnes et al., 1993; Banfield et al., 2004; Wilson et al., 2002).

This area of background error is largely captured by the ensemble spread and the values of the spread match up well with the background error (Fig. 7a). The ensemble spread is seen to be largest around 45°N and the shape of the spread is spatially similar to that of the analysis error. The average analysis error is slightly smaller than the background error and the analysis spread has the same spatial structure as the analysis error (Fig. 7b) along the temperature front. There is a patch of larger analysis error near the pole which is not well captured by the ensemble spread.

Full coverage observation experiments are an excellent method of studying predictability and testing the performance of the

Please cite this article in press as: Hoffman, M.J., et al. An ensemble Kalman filter data assimilation system for the martian atmosphere: Implementation and simulation experiments. Icarus (2010), doi:10.1016/j.icarus.2010.03.034

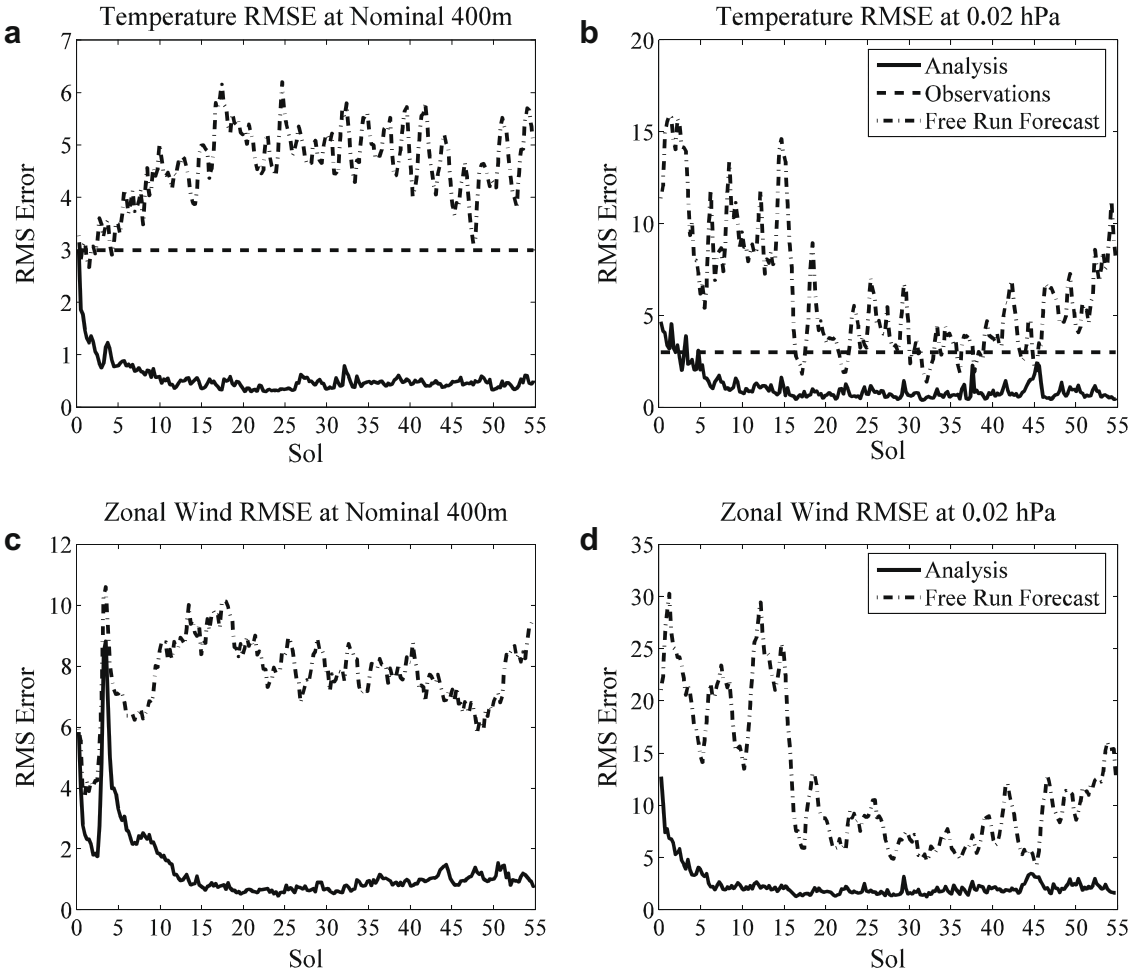

Fig. 9. Temperature RMS error north of 30°N from an experiment using simulated TES retrievals with 3 K error, 10% inflation, and a 16 member ensemble at (top left) a nominal height of 400 m above ground level and (top right) 0.02 hPa height. Zonal wind RMS error north of 30°N from the same at (bottom left) a nominal height of 400 m above ground level and (bottom right) 0.02 hPa height.

LETKF, however they do not represent the actual distribution of the TES retrieval data. To investigate the sensitivity of the LETKF–MGCM system to data coverage, the simulated TES retrievals are used. We note that the number of simulated TES retrievals is less than 7% of the number of observations for the full coverage experiments.

The state estimate of temperature in the simulated TES retrieval experiment is worse than the analysis using full coverage observations, although both experiments reach very low RMS error levels after 10–15 sols (Fig. 8a). Having observations at every grid point leads to a quicker initial reduction of the temperature error: the analysis error drops below the observation error after just 1 assimilation in the full coverage case and after 2 assimilations in the simulated TES case. The state estimates of zonal velocity (Fig. 8b) and meridional velocity (Fig. 8c) exhibit similar behavior. There is a spike in analysis error during the first five sols of the both experiments. After that initial period, the analysis error drops dramatically and approaches an asymptotic value between 13 and 14 sols.

As in the full coverage experiments, the error reduction exhibits different behavior at 0.02 hPa and at a nominal 400 m height above ground level. In addition to the difference in dynamics that affected the results in the full coverage experiments, here 0.02 hPa height never includes simulated TES retrievals and a nominal height of 400 m above ground rarely does so nearly all corrections at these two levels come from observations at other levels. The temperature RMS error in both levels decreases below the observation RMS error, but the state estimate for a nominal 400 m above ground is more accurate when compared to the free run forecast (Fig. 9). The zonal wind analysis state estimate in both levels is also improved over the free run (Fig. 9). The assimilation provides a significant immediate improvement in the upper levels of the model. After five sols, the analysis RMS error at 0.02 hPa height is approximately 4 m/s, while the free run error is approximately 17 m/s. The analysis RMS error at 0.02 hPa appears to approach an asymptote at approximately 1 m/s, while the free run forecast RMS error fluctuates from 5 m/s to 10 m/s. At a nominal height of 400 m above ground, the free run forecast error remains approximately 5 m/s throughout the simulation, while the analysis RMS error drops to approximately 0.8 m/s.

Analysis errors are higher in the upper atmosphere using the simulated TES retrievals because the internal dynamics play a relatively more important role compared to forcing than in the lower atmosphere and there are no observations higher than 0.1 hPa. In contrast to the full coverage observation experiment (Fig. 6b), where the dominant vertical errors were from the baroclinic waves in the lower atmosphere, the dominant analysis errors using simulated TES retrievals are in the zonal jet in the upper levels of the winter hemisphere (Fig. 10). The state estimate at a nominal 400 m height above ground is accurate, even in the absence of direct observations, because the surface forcing constrains the atmosphere in the lower levels.

Despite the presence of analysis error in the upper atmosphere at 0.02 hPa, the analysis provides a superior estimate of the location and strength of the zonal jet than the free run forecast

Please cite this article in press as: Hoffman, M.J., et al. An ensemble Kalman filter data assimilation system for the martian atmosphere: Implementation and simulation experiments. Icarus (2010), doi:10.1016/j.icarus.2010.03.034

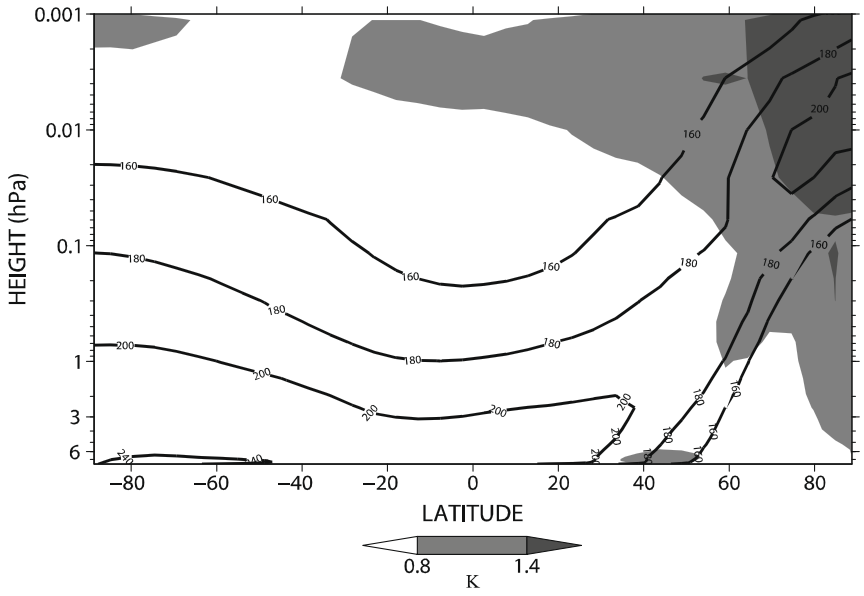

Fig. 10. Vertical profile of the analysis RMS error [K] (shaded) and average truth temperature field [K] from sol 2 to sol 21 of the simulation (contour) using simulated TES retrievals with 3 K observation error, 10% inflation, and 16 ensemble members. The vertical axis is labeled by reference pressure in hPa, plotted with a log axis. Note that there is a change in the colorbar scale relative to Fig. 6b.

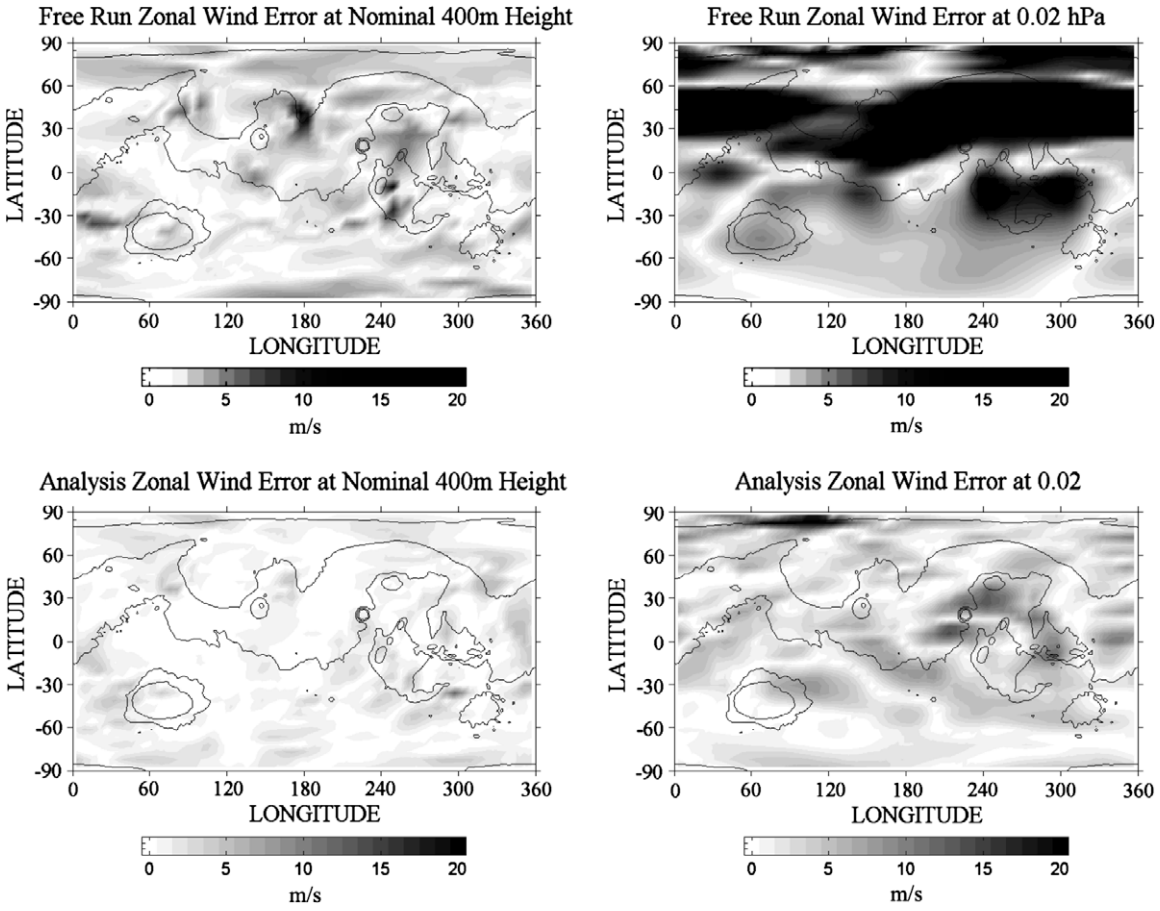

Fig. 11. Magnitude of the error in the free run forecast of zonal wind [m/s] at a nominal height of 400 m above ground level (top left) and 0.02 hPa height (top right) and the analysis of zonal wind [m/s] at a nominal height of 400 m above ground level (bottom left) and 0.02 hPa height (bottom right) from sol 2, 6 h of the experiment using simulated TES retrievals with error 3 K, 16 ensemble members, and 10% inflation.

(Fig. 11). After two sols, the free run forecast has an incorrect location for the Northern Hemisphere zonal jet, which leads to errors of over 20 m/s. In the analysis, the jet location is correct, and errors are less than 10 m/s in the jet region. Improvement in the zonal wind is also seen near the surface at a nominal 400 m height above ground, but is not as dramatic as in the upper atmosphere.

Please cite this article in press as: Hoffman, M.J., et al. An ensemble Kalman filter data assimilation system for the martian atmosphere: Implementation and simulation experiments. Icarus (2010), doi:10.1016/j.icarus.2010.03.034

6. Summary

The local ensemble transform Kalman filter (LETKF) applied to the GFDL Mars general circulation model (MGCM) in perfect model experiments assimilating only temperature data results in a significant reduction in the RMS error of the temperature and wind fields as compared to a forecast with no data assimilation. The martian atmospheric dynamics are dominated by solar heating and topographic forcing at lower levels and the primary sources of analysis error are the large scale, low wavenumber baroclinic waves in the winter hemisphere. These sources of error are accurately captured by the ensemble spread. The atmosphere is more dynamically driven in the upper levels and characterized by a strong zonal jet which the LETKF analysis accurately corrects, even without any wind observations. Assimilations using observations at every grid point provide a good test of the LETKF–MGCM system, but the real observational data coverage from the TES instrument is sparse (only 7% of the full coverage) and has vertically correlated errors. The vertical correlation in the observation errors was not accounted for in these experiments and larger random errors were used instead. To see the sensitivity of the system to the decreased observation density of satellite retrievals, retrievals are simulated at the grid points closest to the real TES track. The resulting analysis is a major improvement over the free run forecast and exhibits similar asymptotic behavior to the full coverage experiment after approximately 15 sols. The full coverage experiment RMS errors asymptote at approximately 0.1 K, while the simulated TES retrieval experiment RMS errors asymptote at approximately 0.3 K, which is a tenth of the 3 K observation error. These results show that there is much potential for using the LETKF–MGCM system to produce an accurate reanalysis of the martian climate. Most of the simulated TES retrievals are at the middle levels of the model, with no retrievals at the upper six levels. As a result, the largest analysis errors using the simulated TES retrievals are in the zonal jet and the upper atmosphere.

The excellent Mars OSSE results obtained here suggest that the MGCM–LETKF system should be capable of assimilating real TES retrievals. The main challenges we expect in the real data case are that the model is far from perfect, and that TES retrievals have poorly known and strongly correlated errors. We plan to address these difficulties with new techniques developed to estimate observation errors and physical parameters (such as parameters needed to model dust lifting) within the LETKF (e.g., Li et al., 2009) and to test the direct assimilation of radiances.

Acknowledgments

This work was supported by the NASA Mars Data Analysis Program (MDAP) Grant NNX07AN97G and the NASA Mars Fundamental Research Program (MFRP) Grant NNX07AV45G.

References

Banfield, D., Ingersoll, A., Keppenne, C., 1995. A steady-state Kalman filter for assimilating data from a single polar-orbiting satellite. J. Atmos. Sci. 52, 737–775.

Banfield, D., Conrath, B.J., Gierasch, P.J., Wilson, R.J., Smith, M.D., 2004. Traveling waves in the martian atmosphere from MGS TES nadir data. Icarus 170 (2). doi:10.1016/j.icarus.2004.03.015.

Barnes, J.R., Pollack, J.B., Haberle, R.M., Leovy, C.B., Zurek, R.W., Lee, H., Schaeffer, J., 1993. Mars atmospheric dynamics as simulated by the NASA Ames general circulation model. 2. Transient baroclinic eddies. J. Geophys. Res. 98, 3125–3148.

Basu, S., Richardson, M.I., Wilson, R.J., 2004. Simulation of the martian dust cycle with the GFDL Mars GCM. J. Geophys. Res. 109, E11906. doi:10.1029/2004JE002243.

Basu, S., Wilson, R.J., Richardson, M.I., Ingersoll, A.P., 2006. Simulation of spontaneous and variable global dust storms with the GFDL Mars GCM. J. Geophys. Res. 111, E09004. doi:10.1029/2005JE002660.

Conrath, B.J., Pearl, J.C., Smith, M.D., Maguire, W.C., Dason, S., Kaelberer, M.S., Christensen, P.R., 2000. Mars Global Surveyor Thermal Emission Spectrometer (TES) observations: Atmospheric temperatures during aerobraking and science phasing. J. Geophys. Res. 105 (E4), 9509–9519.

Hinson, D., Wilson, R.J., 2004. Temperature inversions, thermal tides, and water ice clouds in the martian tropics. J. Geophys. Res. 109, E01002. doi:10.1029/JE002129.

Hinson, D.P., Wilson, R.J., Smith, M.D., Conrath, B.J., 2003. Stationary planetary waves in the atmosphere of Mars during southern winter. J. Geophys. Res. 108 (E1), 5004. doi:10.1029/2002JE001949.

Hoffman, R.N., Ponte, R.M., Kostelich, E.J., Blumberg, A., Szunyogh, I., Vinogradov, S., Henderson, J.M., 2008. A simulation study using a local ensemble transform Kalman filter for data assimilation in New York Harbor. J. Atmos. Oceanic Technol. 25, 1638–1656.

Houben, H., 1999. Assimilation of Mars Global Surveyor meteorological data. Adv. Space Res. 23 (11), 1899–1902.

Hunt, B.R., Kostelich, E.J., Szunyogh, I., 2007. Efficient data assimilation for spatiotemporal chaos: A local ensemble transform Kalman filter. Physica D 230, 112–126.

Kahre, M.A., Murphy, J.R., Haberle, R.M., 2006. Modeling the martian dust cycle and surface dust reservoirs with the NASA Ames general circulation model. J. Geophys. Res. 111, E06008. doi:10.1029/2005JE002588.

Kahre, M.A., Hollingsworth, J.L., Haberle, R.M., Murphy, J.R., 2008. Investigations of the variability of dust particle sizes in the martian atmosphere using the NASA Ames general circulation model. Icarus 195 (2), 576–597. doi:10.1016/j.icarus.2008.01.023.

Lewis, S.R., Read, P.L., 1995. An operational data assimilation scheme for the martian atmosphere. Adv. Space Res. 16 (6), 9–13.

Lewis, S.R., Collins, M., Read, P.L., 1996. Martian atmospheric data assimilation with a simplified general circulation model: Orbiter and lander networks. Planet. Space Sci. 44, 1395–1409.

Lewis, S.R., Collins, M., Read, P.L., 1997. Data assimilation with a martian atmospheric GCM: An example using thermal data. Adv. Space Res. 19, 1267–1270.

Lewis, S.R., Read, P.L., Conrath, B.J., Pearl, J.C., Smith, M.D., 2007. Assimilation of Thermal Emission Spectrometer atmospheric data during the Mars Global Surveyor aerobraking period. Icarus 192, 327–347.

Li, H., Kalnay, E., Miyoshi, T., 2009. Simultaneous estimation of covariance inflation and observation errors within ensemble Kalman filter. Q. J. R. Meteorol. Soc. 134 (639), 523–533.

Lin, S.-J., 1997. A finite-volume integration method for computing pressure gradient forces in general vertical coordinates. Q. J. R. Meteorol. Soc. 123, 1749–1762.

Lin, S.-J., 2004. A "vertically Lagrangian" finite-volume dynamical core for global models. Mon. Weather Rev. 132, 2293–2307.

Lin, S.-J., Rood, R.B., 1996. Multidimensional flux-form semi-Lagrangian transport schemes. Mon. Weather Rev. 124, 2046–2070.

Lin, S.-J., Rood, R.B., 1997. An explicit flux-form semi-Lagrangian shallow water model on the sphere. Q. J. R. Meteorol. Soc. 123, 2477–2498.

Lorenc, A.C., Bell, R.S., Macpherson, B., 1991. The Meteorological Office analysis correction data assimilation scheme. Q. J. R. Meteorol. Soc. 117, 59–89.

Montabone, L., Lewis, S.R., Read, P.L., 2005. Interannual variability of martian dust storms in assimilation of several years of Mars Global Surveyor observations. Adv. Space Res. 36, 2146–2155.

Montabone, L., Lewis, S.R., Read, P.L., Hinson, D.P., 2006. Validation of martian meteorological data assimilations for MGS/TES using radio occultation measurements. Icarus 198, 113–232. doi:10.1016/j.icarus.2006.07.012.

Ockert-Bell, M.E., Bell III, J.F., Pollack, J.B., McKay, C.P., Forget, F., 1997. Absorption and scattering properties of the martian dust in the solar wavelengths. J. Geophys. Res. 102, 9039–9050.

Putnam, W.M., Lin, S.-J., 2007. Finite-volume transport on various cubed-sphere grids. J. Comput. Phys. 227 (1), 55–78.

Read, P.L., Lewis, S.R., 2004. The Mars Climate Revisited: Atmosphere and Environment of a Desert Planet. Springer-Praxis.

Richardson, M.I., Wilson, R.J., 2002. Investigation of the nature and stability of the martian seasonal water cycle with a general circulation model. J. Geophys. Res. 107 (E5), 5031. doi:10.1029/2001JE001536.

Richardson, M.I., Wilson, R.J., Rodin, A.V., 2002. Water ice clouds in the martian atmosphere: General circulation model experiments with a simple cloud scheme. J. Geophys. Res. 107 (E9), 5064. doi:10.1029/2001JE001804.

Smith, M.D., Pearl, J.C., Conrath, B.J., Christensen, P.R., 2000. Mars Global Surveyor Thermal Emission Spectrometer (TES) observations of dust opacity during aerobraking and science phasing. J. Geophys. Res. 105 (E4), 9539–9552.

Smith, M.D., Pearl, J.C., Conrath, B.J., Christensen, P.R., 2001. Thermal Emission Spectrometer results: Mars atmospheric thermal structure and aerosol distribution. J. Geophys. Res. 106 (E10), 23929–23945.

Szunyogh, I., Kostelich, E.J., Gyarmati, G., Kalnay, E., Hunt, B.R., Ott, E., Satterfield, E., Yorke, J.A., 2005. Assessing a local ensemble Kalman filter: Perfect model experiments with the National Centers for Environmental Prediction Model. Tellus 57A, 528–545.

Szunyogh, I., Kostelich, E.J., Gyarmati, G., Kalnay, E., Hunt, B.R., Ott, E., Satterfield, E., Yorke, J.A., 2008. A local ensemble transform Kalman filter data assimilation system for the NCEP global model. Tellus 60A, 113–130.

Toon, O.B., McKay, C.P., Ackerman, T.P., Santhanam, K., 1989. Rapid calculation of radiative heating rates and photodissociation rates in inhomogeneous multiple scattering atmospheres. J. Geophys. Res. 94, 16287–16301.

Whitaker, J.S., Hamill, T.M., Wei, X., Song, Y., Toth, Z., 2008. Ensemble data assimilation with the NCEP Global Forecast System. Mon. Weather Rev. 136, 463–482.

Please cite this article in press as: Hoffman, M.J., et al. An ensemble Kalman filter data assimilation system for the martian atmosphere: Implementation and simulation experiments. Icarus (2010), doi:10.1016/j.icarus.2010.03.034

Wilson, R.J., Hamilton, K.P., 1996. Comprehensive model simulation of thermal tides in the martian atmosphere. J. Atmos. Sci. 53 (9), 1290–1326.

Wilson, R.J., Banfield, D., Conrath, B.J., Smith, M.D., 2002. Traveling waves in the Northern Hemisphere of Mars. Icarus 29 (14). doi:10.1029/2002GL014866.

Wilson, R.J., Neumann, G., Smith, M.D., 2007. The diurnal variation and radiative influence of martian water ice clouds. Geophys. Res. Lett. 34, L02710. doi:10.1029/2006GL027976.

Wilson, R.J., Lewis, S.R., Montabone, L., 2008a. Influence of water ice clouds on martian tropical atmospheric temperatures. Geophys. Res. Lett. 35, L07202. doi:10.1029/2007GL032405.

Wilson, R.J., Haberle, R.M., Noble, J., Bridger, A.F.C., Schaeffer, J., Barnes, J.R., Cantor, B.A., 2008b. Simulation of the 2001 planet-encircling dust storm with the NASA/NOAA Mars general circulation model. LPI contributions No. 1447, p. 9023.

Wolff, M.J., Clancy, R.T., 2003. Constraints on the size of martian aerosols from Thermal Emission Spectrometer observations. J. Geophys. Res. 108 (E9), 5098. doi:10.1029/2003JE002058.

Zhang, K.Q., Ingersoll, A.P., Kass, D.M., Pearl, J.C., Smith, M.D., Conrath, B.J., Haberle, R.M., 2001. Assimilation of Mars Global Surveyor atmospheric temperature data into a general circulation model. J. Geophys. Res. 106 (E12), 32863–32877.

Please cite this article in press as: Hoffman, M.J., et al. An ensemble Kalman filter data assimilation system for the martian atmosphere: Implementation and simulation experiments. Icarus (2010), doi:10.1016/j.icarus.2010.03.034